



Published in final edited form as:

Nature. 2009 June 11; 459(7248): 808–813. doi:10.1038/nature08076.

Alkylated DNA damage flipping bridges base and nucleotide excision repair

Julie L. Tubbs¹, Vitaly Latypov², Sreenivas Kanugula³, Amna Butt², Manana Melikishvili⁴, Rolf Kraehenbuehl^{5,†}, Oliver Fleck^{5,‡}, Andrew Marriott², Amanda J. Watson², Barbara Verbeek^{2,§}, Gail McGown², Mary Thorncroft², Mauro F. Santibanez-Koref⁶, Christopher Millington⁷, Andrew S. Arvai¹, Matthew D. Kroeger¹, Lisa A. Peterson⁸, David M. Williams⁷, Michael G. Fried⁴, Geoffrey P. Margison^{2,*}, Anthony E. Pegg^{3,*}, and John A. Tainer^{1,9,*}

¹Skaggs Institute for Chemical Biology and Department of Molecular Biology, The Scripps Research Institute, La Jolla, CA 92037, USA

²Cancer Research UK Carcinogenesis Group, Paterson Institute for Cancer Research, University of Manchester, Manchester, M20 4BX, UK

³Department of Cellular and Molecular Physiology, Milton S. Hershey Medical Center, Pennsylvania State University College of Medicine, Hershey, PA 17033, USA

⁴Center for Structural Biology, Department of Molecular and Cellular Biochemistry, University of Kentucky, Lexington, KY 40536, USA

⁵NWCRF Institute, Bangor University, Gwynedd LL57 2UW, UK

⁶Institute of Human Genetics, University of Newcastle-upon-Tyne, UK

⁷Centre for Chemical Biology, Department of Chemistry, University of Sheffield, UK

⁸Division of Environmental Health Sciences and the Masonic Cancer Center, University of Minnesota, Minneapolis, MN 55455, USA

Users may view, print, copy, and download text and data-mine the content in such documents, for the purposes of academic research, subject always to the full Conditions of use:http://www.nature.com/authors/editorial_policies/license.html#terms

*Correspondence and requests for materials should be addressed to G.P.M. (email: GMargison@picr.man.ac.uk) or A.E.P. (email: aep1@psu.edu) or J.A.T. (email: jat@scripps.edu).

[†]Present address: Cancer Research UK DNA Damage Response Group, Paterson Institute for Cancer Research, University of Manchester, Manchester, UK

[‡]Present address: Department of Biology, University of Copenhagen, Ole Maaløes Vej 5, DK-2200 Copenhagen N, Denmark

[§]Present address: Department of Toxicology, University of Mainz, D-55131 Mainz, Germany.

Author Contributions M.D.K. and J.L.T. purified AtI1 protein and prepared AtI1:oligomer complexes for crystallization. A.S.A. and J.L.T. crystallized AtI1 and collected, processed, and refined X-ray data. O⁶-pobG oligomers were synthesized by L.A.P. for crystallization and by C.M. and D.M.W. for SPR. A.J.W. and B.V. designed and synthesized oligonucleotides that contributed to the SPR data. A.M. and A.J.W. produced and characterized pure AtI1 protein for the SPR analyses. G.M. and M.T. performed SPR analyses. M.M. and M.G.F. performed electrophoretic mobility shift assays and analytical ultracentrifugation experiments and analyzed the results. V.L. and A.B. generated AtI1 single and double deletants and AtI1-complement in *S. pombe* and carried out spot and clonogenic assays. R.K. and O.F. carried out the mutation assays in *S. pombe*. S.K. prepared constructs for and purified AtI1, eATL, NvATL, AGT C145S, UvrA, UvrB, and UvrC, and performed Far Western analyses, AtI1 expression assays in *E. coli*, and ATL inhibition assays. M.F.S.-K. contributed intellectually to the initiation and design of the studies at the Paterson Institute. O.F., G.P.M., A.E.P., and J.A.T. provided intellectual guidance and research support. J.L.T. and J.A.T. wrote the paper. All authors discussed the results and manuscript.

Author Information Atomic coordinates and structure factors for the reported crystal structures have been deposited with the Protein Data Bank under accession codes 3GVA (AtI1), 3GX4 (AtI1:O⁶-mG-DNA), and 3GYH (AtI1:O⁶-pobG-DNA). Reprints and permissions information is available at <http://www.nature.com/reprints>.

⁹Life Sciences Division, Department of Molecular Biology, Lawrence Berkeley National Laboratory, Berkeley, CA 94720, USA

Abstract

Alkyltransferase-like proteins (ATLs) share functional motifs with the cancer chemotherapy target *O*⁶-alkylguanine DNA-alkyltransferase (AGT) and paradoxically protect cells from the biological effects of DNA alkylation damage, despite lacking the AGT reactive cysteine and alkyltransferase activity. Here we determine *S. pombe* ATL structures without and with damaged DNA containing endogenous lesion *O*⁶-methylguanine or cigarette smoke-derived *O*⁶-4-(3-pyridyl)-4-oxobutylguanine. These results reveal non-enzymatic DNA nucleotide flipping plus increased DNA distortion and binding pocket size compared to AGT. Our analysis of lesion-binding site conservation identifies new ATLs in sea anemone and ancestral archaea, indicating ATL interactions are ancestral to present-day repair pathways in all domains of life. Genetic connections to XPG and ERCC1 in *S. pombe* homologs Rad13 and Swi10 and biochemical interactions with UvrA and UvrC combined with structural results reveal that ATLs sculpt alkylated DNA to create a genetic and structural intersection of base damage processing with nucleotide excision repair.

DNA *O*⁶-alkylguanine lesions are mutagenic and cytotoxic: they mis-pair during replication with thymine, resulting in G:C to A:T transition mutations^{1–4}. Human *O*⁶-alkylguanine DNA lesions are repaired by *O*⁶-alkylguanine-DNA alkyltransferase (AGT), also known as *O*⁶-methylguanine-DNA methyltransferase (MGMT), which transfers guanine *O*⁶-alkyl adducts to its reactive cysteine reversing damage¹. This prevents mutations but resists alkylating chemotherapies^{2,5}. Active site -PCHRV- motif Cys1456,7 plus Arg128 and Tyr114 nucleotide rotating residues are conserved from bacterial to human AGTs^{1,2,8}. Human AGT (hAGT) structures alone^{9,10} and with small molecule⁹ or DNA^{11,12} substrates showed how AGT promotes resistance to anticancer therapies by directly reversing DNA guanine alkylation damage.²

Recently bacterial and yeast proteins with sequence similarity to the AGT DNA-binding domain were identified with the Cys alkyl acceptor replaced by tryptophan, alanine, or another residue,¹³ and hence named alkyltransferase-like proteins (ATLs). ATLs from *S. pombe* (Atl1) and *E. coli* (eAtl) inhibit *O*⁶-methylguanine (*O*⁶-mG) repair by hAGT^{14,15}. eAtl also binds abasic site-containing dsDNA,¹⁶ and Atl1 binds ssDNA containing *O*⁶-methyl-, *O*⁶-benzyl-, *O*⁶-(4-bromophenyl)- or *O*⁶-hydroxyethyl-guanine. Yet, ATLs do not cleave the alkyl group, base, or oligonucleotide near the lesion^{14,15}, and eAtl Trp to Cys mutation does not restore alkyltransferase activity¹⁴. As *S. pombe* and *T. thermophilus* lack AGT, and inactivation of their ATL genes, *atl1* and *TTHA1564*, respectively^{15,17}, reduces their alkylation damage resistance, ATLs protect against biological effects of DNA alkylation damage by an undefined mechanism.

Tight binding affinities^{16,17} for and inability to repair^{14,15} *O*⁶-alkyl lesions implied ATLs are damage sensors or act in nucleotide excision repair (NER)^{13,15}, which excises bulky, DNA-distorting lesions. However, lack of structures, persuasive evidence, or specific mechanism has obscured how ATL ameliorates DNA damage effects. To clarify this

protection, we combined structural, biochemical, and genetic experiments on AtI1 from the fission yeast *S. pombe*. Our results reveal ATL binding generates a stable complex that sculpts alkylated DNA base damage for NER pathway entry.

AtI1 structure and lesion binding

To characterize AtI1-DNA damage interactions, we crystallized and solved structures to 2.0, 2.7, and 2.8 Å resolution, respectively, for AtI1 alone (Fig. 1a and Supplementary Table 1) and in complex with oligonucleotides containing either O^6 -mG (Fig. 1b, d and Supplementary Table 1) or O^6 -4-(3-pyridyl)-4-oxobutylguanine (O^6 -pobG) (Fig. 1c and Supplementary Table 1), a bulky and toxicologically-relevant adduct¹⁸. AtI1 shares the hAGT catalytic domain fold (superposition root mean square difference = 1.6 Å) (Fig. 1a), including residues required for AGT activity, DNA-binding, and nucleotide flipping. Yet, AtI1 specifically lacks AGT's active site Cys and Asn hinge that couples helix-turn-helix (HTH) DNA binding and active site motifs (Fig. 1a).

AtI1 flips both O^6 -mG (Fig. 1b, d) and O^6 -pobG (Fig. 1c) into a pocket containing -PWHRV- motif Trp56, consistent with fluorescence measured flipping for a base opposite an AP site in eAtI16 and for O^6 -mG in TTHA156417. AtI1 displays no AGT activity,¹⁵ suggesting nucleotide flipping is a switch for pathway activation, not catalysis. To our knowledge, AtI1 (Fig. 1b-d), eAtI16, and TTHA156417 are among the first reported non-enzymatic DNA-binding proteins that flip nucleotides. Our AtI1 structures show ATL rotates nucleotides into a specificity pocket. Arg39 intercalates the DNA base stack (Fig. 1d) and hydrogen bonds the orphaned cytosine, thereby stabilizing the extra-helical alkylguanine. Trp56, rather than AGT Cys, is evident in electron density omit maps (Fig. 1a), acting in hydrophobic packing with the alkyl group (Fig. 1c, d). Arg69 guanidinium stacks against the alkylguanine base in a cation- π interaction (Fig. 1d).

Alkylguanine base side and main chain hydrogen bonds are conserved from AtI1 to AGT, but the AtI1 lesion-binding pocket is ~three times larger (Supplementary Table 2). Loop residues 65-73 define one wall of the alkyl-binding pocket, adopting a conformation further from the protein core than in AGT, thereby enlarging the pocket (Fig. 1a and Fig. 2a). Also, lesion-binding pocket Lys45-Pro55 cap is ~5.3 Å further out than the comparable AGT Pro140 (C α to C α distance) that interacts with larger alkyl groups^{9,11,12}. Moreover, ATL Ile71 replaces AGT Tyr158, which would clash with the AtI1 Trp56 side chain in its DNA-bound, closed position.

AtI1's larger cavity explains its broad lesion range that includes O^6 -benzyl-, O^6 -(4-bromophenyl)- or O^6 -hydroxyethyl-guanine. In the O^6 -pobG-DNA complex structure, the pob group is wedged between Pro50 and Trp56, making only these hydrophobic protein interactions (Fig. 1c). No major changes in lesion-binding site, or DNA conformation occur between O^6 -mG- and O^6 -pobG-bound AtI1. Pob would push against the active (or binding) site loop in the smaller AGT active site, explaining why AGT repairs pob lesions at a decreased rate compared to O^6 -mG¹⁹. Pob adopts a conformation incompatible with smaller *E. coli* AGT (Ada-C and Ogt) active site pockets, consistent with its poor repair by Ada-C and Ogt²⁰ and need for ATLS for bulky adducts in organisms like *E. coli*.

AtI1 DNA-binding

Like AGT, AtI1 uses an HTH motif to bind the DNA minor groove (Fig. 1b and Fig. 2a). All damaged-strand contacts are to alkylguanine and two 3'-adjacent nucleotide phosphate groups (Fig. 2d). DNA binding site loop (Ser67 and Lys70) and loop (Thr92 and Ser93) residues form DNA contacts not found in AGT. AtI1 DNA-binding buries $\sim 1050 \text{ \AA}^2$ versus 788 \AA^2 of AGT buried surface area, consistent with tighter DNA binding^{16,17}.

AtI1 bends DNA by $\sim 45^\circ$ (Fig. 2a), whereas AGT only bends DNA $\sim 30^\circ$ ¹¹. AtI1 achieves greater DNA bending through synergistic N-terminus and binding site loop actions. The AtI1 N-terminal helix extends outward more than the corresponding AGT helix, which follows a loop leading toward the N-terminal domain (Fig. 1a and Fig. 2a). This N-terminal extension pushes against the phosphate backbone of the complementary strand opposite the flipped nucleotide. Moreover, the binding site loop acts as a gate that switches between "open" (Fig. 2b) and "closed" (Fig. 2c) conformations of free and DNA-bound AtI1, respectively, with flanking glycines suggesting flexibility. This "gating" action was proposed in AGT computational simulations²¹, but not seen in crystal structures^{11,12}. The AtI1 binding site loop open-to-closed conformational switch appears suitable to play an active role in signalling by shifting covering Arg and Ile side chains to expose the C-terminal loop for possible intermolecular interactions.

If the closed, bent ATL-DNA complex is a platform for repair protein recognition, then we expect the complex to be stable; yet, K_D was estimated by gel-shift as only 0.41 \mu M for TTHA1564 with O^6 -mG17. To test binding affinity, we measured AtI1 binding and dissociation to and from oligonucleotides containing O^6 -mG, O^6 -pobG, or abasic site by surface plasmon resonance (Fig. 3a). AtI1 binding to oligonucleotides containing alkylG was $0.02\text{--}0.3 \text{ nM}$, but binding to abasic site dsDNA was low and/or transient (Fig. 3a). Langmuir fit with mass transfer limitation indicates $k_{ass} = 1.21 \times 10^{-7} \pm 0.20 \times 10^{-7} \text{ M}^{-1}\text{s}^{-1}$; $k_{diss} = 0.004 \pm 0.0006 \text{ s}^{-1}$ and $K_D = 0.35 \pm 0.04 \text{ nM}$ for O^6 -mG and $k_{ass} = 2.20 \times 10^{-7} \pm 0.56 \times 10^{-7} \text{ M}^{-1}\text{s}^{-1}$; $k_{diss} = 0.0003 \pm 0.00002 \text{ s}^{-1}$ and $K_D = 0.016 \pm 0.004 \text{ nM}$ for O^6 -pobG. Thus, while "on" rates were similar for both lesions, the "off" rate for pob oligonucleotide was slower: higher affinity (K_D) for the pob oligonucleotide shows larger O^6 -alkyl groups are accommodated stably.

We also measured AtI1 binding to methylated double-strand oligonucleotides by gel-shift (Fig. 3b and Supplementary Fig. 1 and Supplementary Table 3) and verified saturated complex stoichiometries by sedimentation equilibrium analysis (Fig. 3c and Supplementary Table 3). Dominant complexes for 13-mer oligonucleotides in solution have 1:1 stoichiometry (Fig. 3b, c and Supplementary Table 3), consistent with our crystal structures, whereas 16-mers form 2:1 limiting complexes (Supplementary Fig. 1a and Supplementary Table 3) and 26-mers form 3:1 limiting complexes (Supplementary Fig. 1b and Supplementary Table 3). Saturated AtI1-nonmethylated DNA complex is formed without intermediate accumulation, suggesting cooperative binding to nonmethylated DNA. DNAs containing O^6 -mG form 1:1 complexes before proceeding to saturation in an additional concerted step, suggesting specific binding to O^6 -mG sites precedes build-up of cooperative assembly, consistent with the open-to-closed switch and a binding site size of ~ 8 bp. This

differs from AGT's binding site size of 4 bp/protein²², possibly due to AGT's added N-terminal domain and the open-to-closed switch (not seen in AGT) that exposes the C-terminal loop.

Atl1 connections to NER

ATLs tightly bind oligonucleotides containing *O*⁶-alkylguanine and switch conformation to expose the C-terminal loop, suggesting ATL-DNA complex binding partners are possible, *in vivo*. In fact, NER protein UvrA interacts with TTHA156417. Similarly, far-western analysis reveals eAtl interacts with *E. coli* NER proteins UvrA and UvrC *in vitro* (Fig. 4a). *E. coli* DNA repair helicase IV (HelD) is also a potential eAtl binding partner¹⁶. Interestingly, *S. pombe* Atl1 interacts with *E. coli* UvrA *in vitro* (Fig. 4b), suggesting ATLs conserve features across species for NER recognition.

To test for Atl1 functional genetic interactions with the NER pathway in fission yeast, we analyzed *S. pombe atl1* and *rad13* (NER pathway XPG endonuclease human homolog which cuts 3' of DNA lesions²³) single and double deletants. We measured Atl1's ability to protect cells from MNNG-induced and spontaneous mutations (Fig. 4c–e). MNNG sensitivity of *atl1* cells was complemented by a plasmid harbouring *atl1* (Supplementary Fig. 2), indicating observed cellular phenotypes are due to *atl1* deletion. Atl1 inactivation causes ~9-fold increased reversion rate of the *ade6-485* mutation, similar to the *rad13* mutant (Fig. 4c top). The MNNG-induced mutation rate is not further increased in the *atl1 rad13* double mutant, revealing an epistatic relationship between Atl1 and Rad13 (Fig. 4c top). These results are supported by spot tests (Fig. 4d) and clonogenic assays (Fig. 4e) indicating Atl1 and Rad13 are also epistatic for MNNG toxicity.

Strikingly, increased spontaneous mutation rate of *rad13* cells is suppressed to wild-type levels by additional Atl1 inactivation (Fig. 4c bottom). This effect is not due to decreased cell survival, as all mutants tested here are viable (Supplementary Fig. 3). Clonogenic assays also revealed Atl1 is epistatic with *S. pombe* Swi10 (Fig. 4f), but not Rhp14 (Fig. 4g) or Rad2 (Fig. 4h) (homologs of human ERCC1, XPA and Fen-1, respectively), for MNNG toxicity. The non-epistatic relationship between Atl1 and Rhp14 suggests Rhp14 has an NER-independent function in response to MNNG, consistent with Rhp14 responses to other DNA damaging agents (R.K. and O.F., unpublished data). As Rad2 plays a role in long-patch base excision repair (BER)²⁴ and the alternative UV excision repair²⁵, lack of epistasis between *atl1* and *rad2* implies the two proteins work in different pathways. *Rad13* and *swi10* mutant phenotypes may reflect build-up of stable hard-to-repair ATL-complex intermediates in the absence of these NER proteins, suggesting ATL-DNA complexes may block alternative repair. Similarly, Atl1 protects *E. coli* cells against MNNG-induced alkylation damage (Supplementary Table 4). Thus, both microbial and eukaryotic genetic evidence suggests ATL bridges DNA-alkylation base damage responses to NER.

Identification of novel ATLs

To see if our structures may characterize other ATLs, we mapped sequence conservation of 197 ATL sequences based upon the Atl1 structure (Supplementary Fig. 4 and Supplementary Fig. 5). For all ATLs, the most conserved residues line the lesion-binding

pocket or act in DNA binding in our structures, suggesting our AtI1 structures are paradigmatic for ATLS.

Significantly, our structure-based sequence analyses helped us identify here the first ATL from any multicellular organism, the recently sequenced starlet sea anemone *Nematostella vectensis*²⁶ plus two archaeal ATLS from *Candidatus Korarchaeum cryptofilum*²⁷ and *Nanoarchaeum equitans*²⁸, ancestral to the two established phyla of archaea (Genbank accession numbers XM_001618690, YP_001736655, and NP_963633, respectively; Supplementary Fig. 4 and Supplementary Fig. 6). We verified *N. vectensis* ATL blocks alkyltransferase activity of hAGT (Supplementary Fig. 7), confirming it is an ATL. The *N. vectensis* genome, which aided in genome characterization of the long-extinct last common ancestor of all eumetazoans, is surprisingly more similar to vertebrates than fruit flies or nematodes²⁶. Therefore, existence of ATL in this multi-cellular eukaryote, plus yeast, bacteria, and ancestral archaea shows ATL is present in all three domains of life and argues ATL was common to evolutionary branches before complex eukaryotes. This discovery suggests higher eukaryotes and mammals will either have an ATL or have lost or replaced it with an analogous protein.

Discussion

Alkylated DNA base damage is classically repaired by direct damage reversal proteins or by lesion-specific DNA glycosylases, which excise modified bases to create abasic sites and initiate the BER pathway²⁹. These base repair processes differ from the versatile NER removal of bulky, unrelated, helix distorting lesions by excising a lesion-containing DNA patch³⁰. Our combined results reveal a general mechanism for ATL to bind weakly distorting *O*⁶-alkylguanine lesions and recruit NER proteins (Fig. 5). We propose ATL binding sculpts alkylguanine into a bulky lesion that is channeled into the NER pathway, explaining NER-mediated repair of *O*⁶-alkylguanine lesions^{31–33}.

ATL may be an unrecognized NER element, with analogues in many organisms, that targets endogenous alkylation damage to NER nucleases. In higher eukaryotes, the NER transcription-coupled repair (TCR) sub-pathway engages downstream damage recognition components of global genome repair (GGR), to effect lesion removal from the transcribed strand³⁴. The NER GGR sub-pathway is initiated by XPC recognition of bulky lesions and, like TCR, results in damage removal by incision on either side of the lesion³⁵. As the *O*⁶-mG lesion is insufficient to block transcription³⁶, ATL binding may stall RNA polymerase to initiate TCR and/or promote lesion processing analogously to DDB2 of mammalian GGR. AtI1-DNA contacts are with the damaged strand, similar to DDB²³⁷, consistent with possible undamaged strand binding by fission yeast XPC homologues Rhp41 or Rhp42, as shown for *S. cerevisiae* XPC orthologue, Rad4³⁸.

ATLS are not alkyltransferases^{14,15,17} or glycosylases^{14,15}, but inhibit AGT^{14,15} (Supplementary Fig. 7). Lack of epistasis for MNNG-induced cell killing between *atl1* and *rad2* shows ATL is not a long-patch BER or alternative UV excision repair protein. Yet, ATL damage recognition resembles AGT and BER glycosylases rather than NER proteins: positive channel for lesion-binding and 180° nucleotide flipping, which allow protein

handoffs without release of toxic and mutagenic DNA intermediates, a hallmark of BER and recombination repair pathways^{39–43}.

ATL binding targets base damage to NER, showing how proteins that bind damage, but do not repair it, may redirect lesion processing.⁴⁴ First, ATL binds base damage analogously to AGT and BER glycosylases^{2,45}, but presents damage to NER similarly to DDB2. Second, in some organisms ATL can block AGT *O*⁶-alkylguanine damage recognition and redirect base repair to NER, constituting a crosstalk pathway connection,⁴⁴ as proposed for AGT^{33,46}, and recently for eATL²⁰. Third, ATL redirects endogenous damage from other repair pathways to NER, as *rad13* mutator is rescued in *atl1 rad13*. Fourth, ancestral archaeal ATL's are ATL-Endo V fusions, suggesting ATL and Endo V act together in a coordinated pathway⁴⁷ with BER nuclease Endo V serving a possible XPG-like function in these organisms, as AGT-Endo V fusion proteins retain both activities⁴⁸. By the Rosetta Stone evolution hypothesis for protein interactions⁴⁷, ATL-Endo V fusions imply ATL provides a primordial connection joining BER and NER. Indeed, recent structures of EndoV⁴⁹ and NER complex DDB1-DDB2³⁷ support such an ancient BER-NER connection by revealing a mutual, wedge-based binding mechanism⁵⁰. Thus, non-enzymatic nucleotide flipping emerges as a surprisingly general mechanism to channel specific base damage into the general damage NER pathway by handoff from a non-enzymatic complex.

Methods Summary

Atl1 purification, crystallization, X-ray diffraction data collection, and structural refinement

C-terminally 6x-His tagged Atl1 was expressed in JM109 cells and purified over Ni-NTA agarose and Superdex 75 columns. Atl1:*O*⁶-mG- and Atl1:*O*⁶-pobG-DNA complexes were prepared at a 1.5:1 DNA:protein molar ratio. Crystals were grown by hanging drop vapor diffusion. Diffraction data were collected at ALS beamline 12.3.1 for Atl1 and at SSRL beamline 11-1 for Atl1:*O*⁶-mG and Atl1:*O*⁶-pobG DNA complexes, and were processed with HKL2000. Structures were solved by molecular replacement with Phaser, using a modified wild-type Ada-C (PDB code 1SFE) as a search model for Atl1, and the refined Atl1 structure as a search model for Atl1:DNA complexes. Crystallographic refinement was done with Crystallography & NMR System (CNS), and Xfit was used for manual model building.

DNA binding by Atl

Oligonucleotide-Atl1 interactions were analyzed by electrophoretic mobility shift assay using standard methods and by surface plasmon resonance with biotinylated *O*⁶-mG-, *O*⁶-pobG-, or AP-site-containing or control oligonucleotides immobilized on a streptavidin-coated surface of a Biacore SA chip and serial dilutions of Atl1 applied to the cell. DNA complex stoichiometries formed under protein saturation conditions were established by sedimentation equilibrium analysis.

Other biochemical assays

AGT inhibition assays performed as described previously. Far western analyses performed by standard methods.

Atl1 expression in *S. pombe*

S. pombe strains originated from GM4 ($h^- atl1::ura4 ura4-D18 leu1-32 his7-366 ade6-M210$), RO131 ($h^+ rad13::kanMX ura4-D18 his3-D1$). MNNG sensitivity determined by agar plate and clonogenic assays. Mutation rates determined as reversions of *ade6-485* to Ade⁺.

Atl1 expression in *E. coli*

pQE-30 empty vector was expressed in *E. coli* GWR109 *ada^- ogt^-* and pQE-30 or pQE-Atl1 in *E. coli* GWR109 *ada^- ogt^- atl^-*. Mutation frequencies determined as number of MNNG-induced Rifampicin resistant mutants (Rif^R) per 10⁸ surviving cells.

Full Methods and any associated references are available in the Supplementary Information of the online version of the paper at www.nature.com/nature.

Supplementary Material

Refer to Web version on PubMed Central for supplementary material.

Acknowledgements

We thank C. C. Vu and J. Gong for aiding in the synthesis of *O*⁶-pobG oligomers, M. N. Boddy, J. Prudden, and A. Sarker for performing genetics and biochemical experiments, G. Guenther, S. Pebernard, R. S. Williams, J. J. Perry, B. R. Chapados, M. Björås, D. S. Shin, K. Hitomi, C. Hitomi, G. Williams, S. Tsutakawa, and P. K. Cooper for helpful suggestions, and the staffs at The Advanced Light Source (ALS) and the Stanford Synchrotron Radiation Laboratory (SSRL). Operations at SSRL and ALS are supported by the U.S. Department of Energy and NIH. This work was supported by National Institutes of Health grants CA097209 (JAT, AEP), GM070662 (MGF), and CA59887 (LAP), North West Cancer Research Fund grant CR675 (OF), Cancer Research-UK (GPM) and CHEMORES (GPM).

References

1. Pegg AE. Repair of *O*⁶-alkylguanine by alkyltransferases. *Mutat. Res.* 2000; 462:83–100. [PubMed: 10767620]
2. Tubbs JL, Pegg AE, Tainer JA. DNA binding, nucleotide flipping, and the helix-turn-helix motif in base repair by *O*⁶-alkylguanine-DNA alkyltransferase and its implications for cancer chemotherapy. *DNA Repair.* 2007; 6:1100–1115. [PubMed: 17485252]
3. Loechler EL, Green CL, Essigmann JM. In vivo mutagenesis by *O*⁶-methylguanine built into a unique site in a viral genome. *Proc. Natl. Acad. Sci. U. S. A.* 1984; 81:6271–6275. [PubMed: 6093094]
4. Pauly GT, Hughes SH, Moschel RC. Comparison of mutagenesis by *O*⁶-methyl- and *O*⁶-ethylguanine and *O*⁴-methylthymine in *Escherichia coli* using double-stranded and gapped plasmids. *Carcinogenesis.* 1998; 19:457–461. [PubMed: 9525280]
5. Margison GP, Santibáñez-Koref MF. *O*⁶-Alkylguanine-DNA alkyltransferase: role in carcinogenesis and chemotherapy. *Bioessays.* 2002; 24:255–266. [PubMed: 11891762]
6. Mitra S, Kaina B. Regulation of repair of alkylation damage in mammalian genomes. *Progr. Nucleic Acid Res. Mol. Biol.* 1993; 44:109–142.
7. Pegg AE, Dolan ME, Moschel RC. Structure, function and inhibition of *O*⁶-alkylguanine-DNA alkyltransferase. *Progr. Nucleic Acid Res. Mol. Biol.* 1995; 51:167–223.
8. Daniels DS, Tainer JA. Conserved structural motifs governing the stoichiometric repair of alkylated DNA by *O*⁶-alkylguanine-DNA alkyltransferase. *Mutat. Res.* 2000; 460:151–163. [PubMed: 10946226]

9. Daniels DS, et al. Active and alkylated human AGT structures: a novel zinc site, inhibitor and extrahelical base binding. *EMBO J.* 2000; 19:1719–1730. [PubMed: 10747039]
10. Wibley JEA, Pegg AE, Moody PCE. Crystal structure of the human O^6 -alkylguanine-DNA alkyltransferase. *Nucleic Acids Res.* 2000; 28:393–401. [PubMed: 10606635]
11. Daniels DS, et al. DNA binding and nucleotide flipping by the human DNA repair protein AGT. *Nat. Struct. Mol. Biol.* 2004; 11:714–720. [PubMed: 15221026]
12. Duguid EM, Rice PA, He C. The structure of the human AGT protein bound to DNA and its implications for damage detection. *J. Mol. Biol.* 2005; 350:657–666. [PubMed: 15964013]
13. Margison GP, et al. Alkyltransferase-like proteins. *DNA Repair.* 2007; 6:1222–1228. [PubMed: 17500045]
14. Pearson SJ, Ferguson J, Santibanez-Koref M, Margison GP. Inhibition of O^6 -methylguanine-DNA methyltransferase by an alkyltransferase-like protein from *Escherichia coli*. *Nucleic Acids Res.* 2005; 33:3837–3844. [PubMed: 16027108]
15. Pearson SJ, et al. A novel DNA damage recognition protein in *Schizosaccharomyces pombe*. *Nucleic Acids Res.* 2006; 34:2347–2354. [PubMed: 16679453]
16. Chen CS, et al. A proteome chip approach reveals new DNA damage recognition activities in *Escherichia coli*. *Nat. Methods.* 2008; 5:69–74. [PubMed: 18084297]
17. Morita R, Nakagawa N, Kuramitsu S, Masui R. An O^6 -methylguanine-DNA methyltransferase-like protein from *Thermus thermophilus* interacts with a nucleotide excision repair protein. *J. Biochem. (Tokyo).* 2008; 144:267–277. [PubMed: 18483064]
18. Wang L, et al. Pyridyloxobutyl adduct O^6 -[4-oxo-4-(3-pyridyl)butyl]guanine is present in 4-(acetoxymethylnitrosamino)-1-(3-pyridyl)-1-butanone-treated DNA and is a substrate for O^6 -alkylguanine-DNA alkyltransferase. *Chem. Res. Toxicol.* 1997; 10:562–567. [PubMed: 9168254]
19. Mijal RS, et al. The repair of the tobacco specific nitrosamine derived adduct O^6 -[4-Oxo-4-(3-pyridyl)butyl]guanine by O^6 -alkylguanine-DNA alkyltransferase variants. *Chem. Res. Toxicol.* 2004; 17:424–434. [PubMed: 15025514]
20. Mazon G, et al. The alkyltransferase-like *ybaZ* gene product enhances nucleotide excision repair of O^6 -alkylguanine adducts in *E. coli*. *DNA Repair.* In Press
21. Hu J, Ma A, Dinner AR. A two-step nucleotide-flipping mechanism enables kinetic discrimination of DNA lesions by AGT. *Proc. Natl. Acad. Sci. U. S. A.* 2008; 105:4615–4620. [PubMed: 18353991]
22. Rasimas JJ, Pegg AE, Fried MG. DNA-binding mechanism of O^6 -alkylguanine-DNA alkyltransferase. Effects of protein and DNA alkylation on complex stability. *J. Biol. Chem.* 2003; 278:7973–7980. [PubMed: 12496275]
23. O'Donovan A, et al. XPG endonuclease makes the 3' incision in human DNA nucleotide excision-repair. *Nature.* 1994; 371:432–435. [PubMed: 8090225]
24. Klungland A, Lindahl T. Second pathway for completion of human DNA base excision-repair: Reconstitution with purified proteins and requirement for DNase IV (FEN1). *EMBO J.* 1997; 16:3341–3348. [PubMed: 9214649]
25. Yonemasu R, et al. Characterization of the alternative excision repair pathway of UV-damaged DNA in *Schizosaccharomyces pombe*. *Nucleic Acids Res.* 1997; 25:1553–1558. [PubMed: 9092661]
26. Putnam NH, et al. Sea Anemone Genome Reveals Ancestral Eumetazoan Gene Repertoire and Genomic Organization. *Science.* 2007; 317:86–94. [PubMed: 17615350]
27. Elkins JG, et al. A korarchaeal genome reveals insights into the evolution of the Archaea. *Proc. Natl. Acad. Sci. U. S. A.* 2008; 105:8102–8107. [PubMed: 18535141]
28. Waters E, et al. The genome of *Nanoarchaeum equitans*: Insights into early archaeal evolution and derived parasitism. *Proc. Natl. Acad. Sci. U. S. A.* 2003; 100:12984–12988. [PubMed: 14566062]
29. Sedgwick B. Repairing DNA-methylation damage. *Nat. Rev. Mol. Cell Biol.* 2004; 5:148–157. [PubMed: 15040447]
30. Hanawalt PC, Spivak G. Transcription-coupled DNA repair: two decades of progress and surprises. *Nat. Rev. Mol. Cell Biol.* 2008; 9:958–970. [PubMed: 19023283]

31. Samson L, Thomale J, Rajewsky MF. Alternative pathways for the *in vivo* repair of O^6 -alkylguanine and O^4 -alkylthymine in *Escherichia coli*: the adaptive response and nucleotide excision repair. *EMBO J.* 1988; 7:2261–2267. [PubMed: 3046938]
32. Voigt JM, Van Houten B, Sancar A, Topal MD. Repair of O^6 -methylguanine by ABC excinuclease of *Escherichia coli in Vitro*. *J. Biol. Chem.* 1989; 264:5172–5176. [PubMed: 2538476]
33. Edara S, Kanugula S, Pegg AE. Expression of the inactive C145A mutant human O^6 -alkylguanine-DNA alkyltransferase in *E. coli* increases cell killing and mutations by N-methyl-N'-nitro-N-nitrosoguanidine. *Carcinogenesis.* 1999; 20:103–108. [PubMed: 9934856]
34. Mellon I. Transcription-coupled repair: a complex affair. *Mutat. Res.* 2005; 577:155–161. [PubMed: 15913669]
35. Branum ME, Reardon JT, Sancar A. DNA repair excision nuclease attacks undamaged DNA. A potential source of spontaneous mutations. *J. Biol. Chem.* 2001; 276:25421–25426. [PubMed: 11353769]
36. Viswanathan A, Doetsch PW. Effects of nonbulky DNA base damages on *Escherichia coli* RNA polymerase-mediated elongation and promoter clearance. *J. Biol. Chem.* 1998; 273:21276–21281. [PubMed: 9694887]
37. Scrima A, et al. Structural Basis of UV DNA-Damage Recognition by the DDB1-DDB2 Complex. *Cell.* 2008; 135:1213–1223. [PubMed: 19109893]
38. Min JH, Pavletich NP. Recognition of DNA damage by the Rad4 nucleotide excision repair protein. *Nature.* 2007; 449:570–575. [PubMed: 17882165]
39. Mol CD, Izumi T, Mitra S, Tainer JA. DNA-bound structures and mutants reveal abasic DNA binding by APE1 and DNA repair coordination. *Nature.* 2000; 403:451–456. [PubMed: 10667800]
40. Chapados BR, et al. Structural basis for FEN-1 substrate specificity and PCNA-mediated activation in DNA replication and repair. *Cell.* 2004; 116:39–50. [PubMed: 14718165]
41. Parikh SS, et al. Uracil-DNA glycosylase-DNA substrate and product structures: Conformational strain promotes catalytic efficiency by coupled stereoelectronic effects. *Proc. Natl. Acad. Sci. U. S. A.* 2000; 97:5083–5088. [PubMed: 10805771]
42. Garcin ED, et al. DNA apurinic-apyrimidinic site binding and excision by endonuclease IV. *Nat. Struct. Mol. Biol.* 2008; 15:515–522. [PubMed: 18408731]
43. Williams RS, et al. Mre11 dimers coordinate DNA end bridging and nuclease processing in double-strand-break repair. *Cell.* 2008; 135:97–109. [PubMed: 18854158]
44. Cline SD, Hanawalt PC. Who's on first in the cellular response to DNA damage? *Nat. Rev. Mol. Cell Biol.* 2003; 4:361–372. [PubMed: 12728270]
45. Hitomi K, Iwai S, Tainer JA. The intricate structural chemistry of base excision repair machinery: Implications for DNA damage recognition, removal, and repair. *DNA Repair.* 2007; 6:410–428. [PubMed: 17208522]
46. Hickman MJ, Samson LD. Role of DNA mismatch repair and p53 in signaling induction of apoptosis by alkylating agents. *Proc. Natl. Acad. Sci. U. S. A.* 1999; 96:10764–10769. [PubMed: 10485900]
47. Marcotte EM, et al. Detecting protein function and protein-protein interactions from genome sequences. *Science.* 1999; 285:751–753. [PubMed: 10427000]
48. Kanugula S, Pauly GT, Moschel RC, Pegg AE. A bifunctional DNA repair protein from *Ferroplasma acidarmanus* exhibits O^6 -alkylguanine-DNA alkyltransferase and endonuclease V activities. *Proc. Natl. Acad. Sci. U. S. A.* 2005; 102:3617–3622. [PubMed: 15731349]
49. Dalhus B, et al. Structures of endonuclease V with DNA reveal initiation of deaminated adenine repair. *Nat. Struct. Mol. Biol.* 2009; 16:138–143. [PubMed: 19136958]
50. Scharer OD, Campbell AJ. Wedging out DNA damage. *Nat. Struct. Mol. Biol.* 2009; 16:102–104. [PubMed: 19190661]

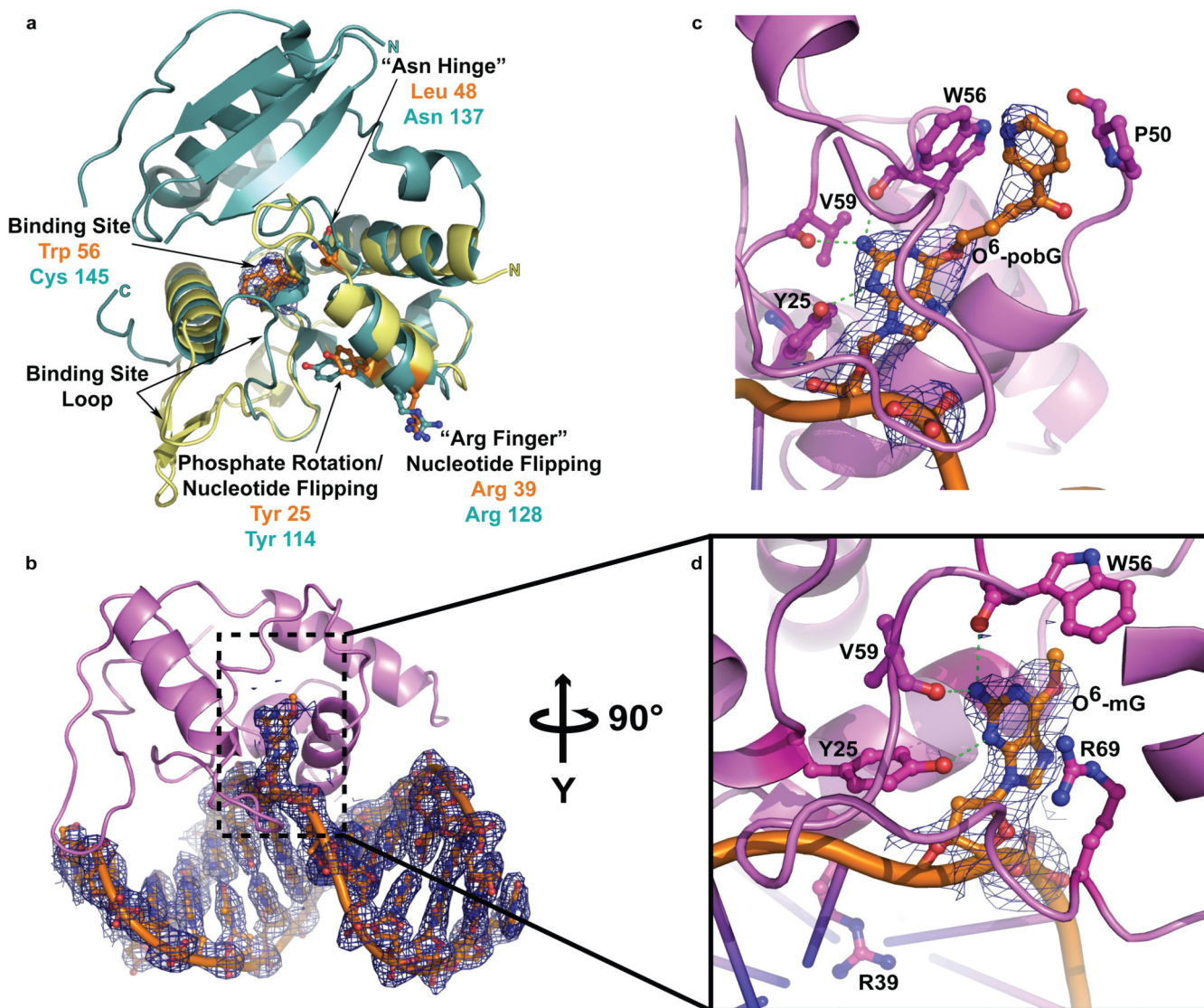


Figure 1. AtI1 structure and lesion-binding site

a, Overlay of AtI1 (yellow) and AGT (cyan; pdb 1EH6) models and comparison of key functional residues. $2F_o - F_c$ electron density (blue) for AtI1 with the binding site Trp56 side chain omitted. **b**, AtI1 (magenta) bound to DNA containing O^6 -mG (orange). $2F_o - F_c$ simulated annealing composite omit map (blue) shown for DNA. **c** and **d**, AtI1 lesion-binding site close-up with O^6 -pobG (**c**) or O^6 -mG (**d**). Amino acid side chains (ball-and-stick) and hydrogen bonds to the damaged guanine (green dashes) show the damage binding.

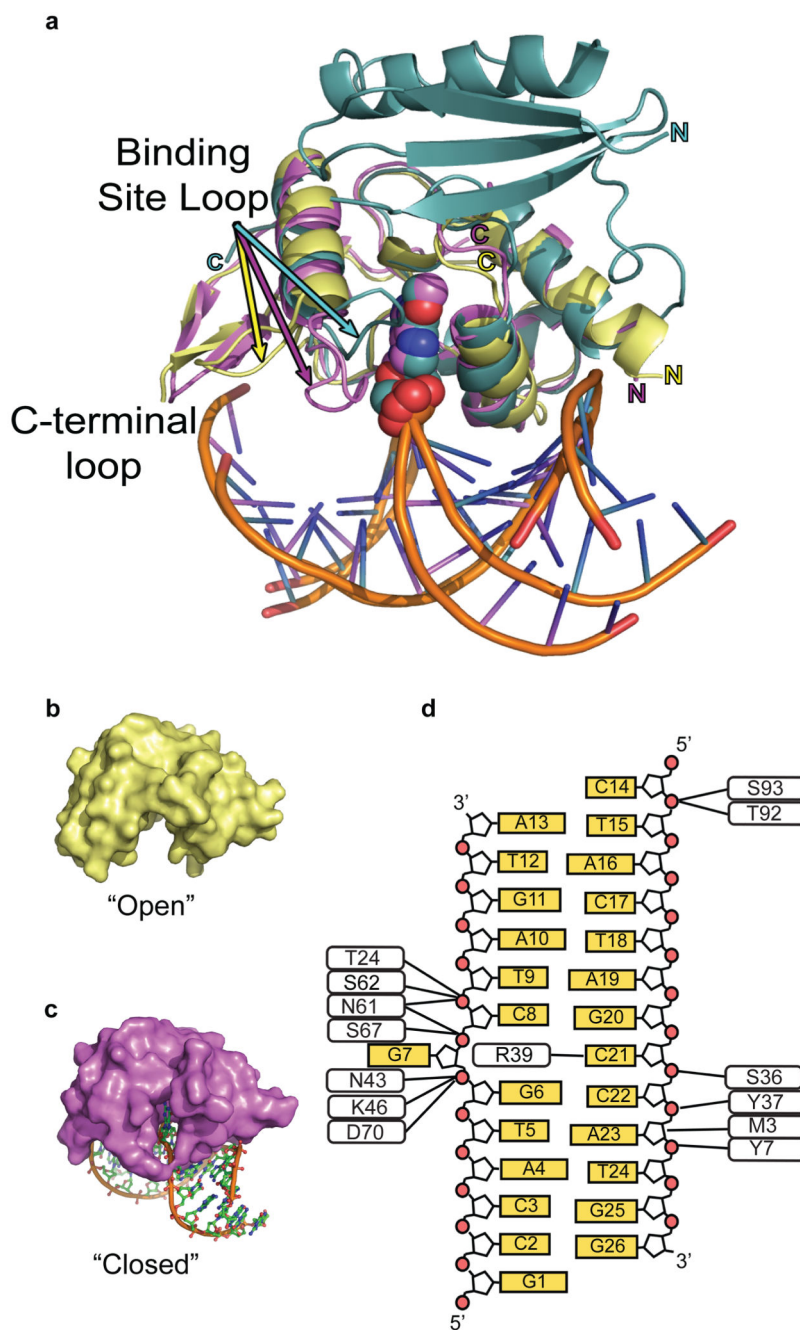


Figure 2. AtI1 DNA binding and damage sculpting

a. Overlay of DNA-free (yellow) and DNA-bound (magenta) AtI1 with the hAGT C-terminal domain (cyan). The rotated O^6 -mG (center, spheres) is shown with the binding site loop that determines the open or closed conformation of AtI1. **b.** AtI1 molecular surface revealing an “open” state. **c.** DNA-bound AtI1 molecular surface showing the protein “closed” state. **d.** AtI1-DNA interaction schematic.

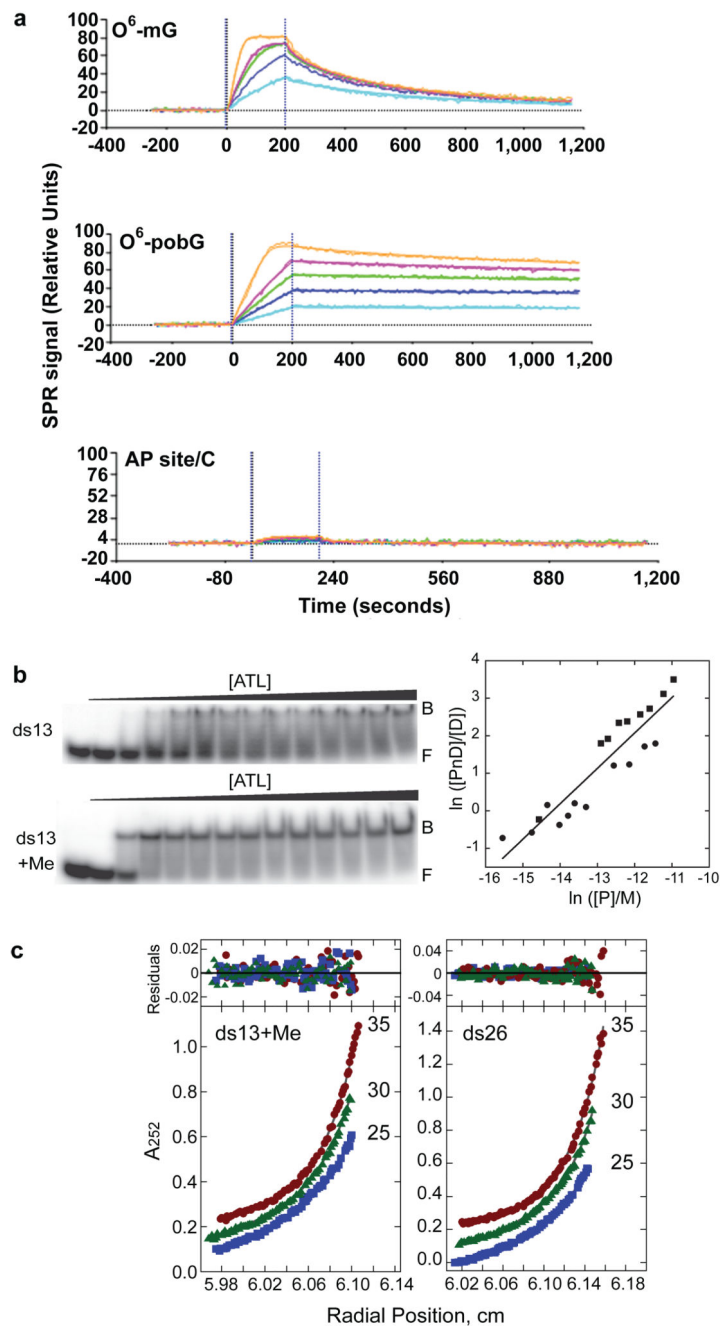


Figure 3. AtI1 DNA lesion binding affinity and stoichiometry

a, AtI1 binding and dissociation for oligonucleotides containing *O*⁶-mG (top), *O*⁶-pobG (center), or abasic site (bottom). **b**, Gel-shift assays for AtI1 binding normal and *O*⁶-mG 13mer dsDNA (left) and associated *O*⁶-mG DNA binding isotherm analysis (right) showing two independent experiments (●, ■). **c**, Sedimentation equilibrium data for *O*⁶-mG 13mer dsDNA complexes (left) and normal 26mer dsDNA (right). Small, randomly distributed residuals (top panels) indicate models in which free protein, DNA, and one protein-DNA

complex equilibrate in solution. Calculated stoichiometries are 1.15 ± 0.08 for O^6 -mG ds13mer and 3.03 ± 0.20 for normal ds26mer.

Author Manuscript

Author Manuscript

Author Manuscript

Author Manuscript

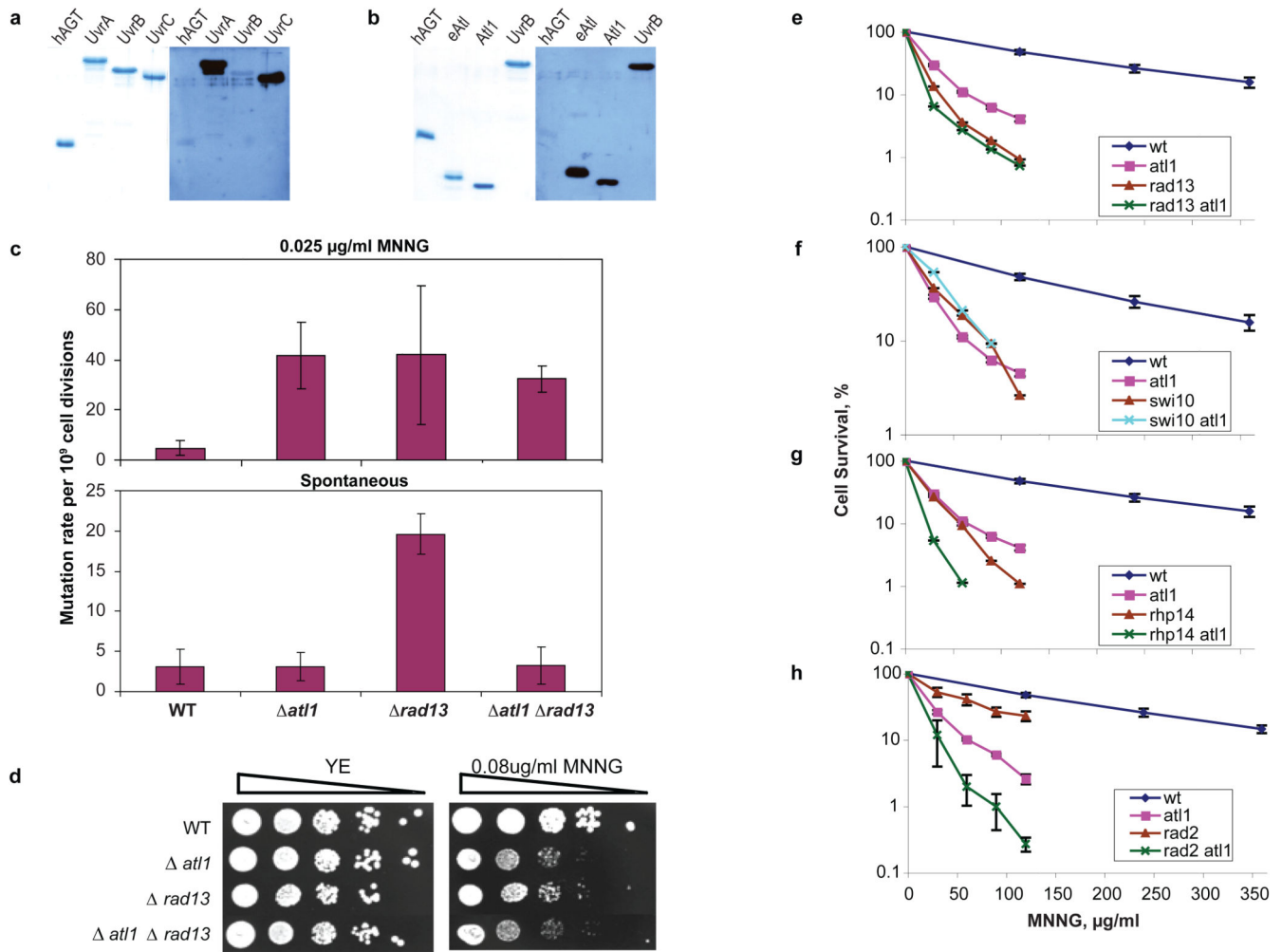
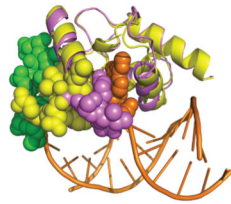


Figure 4. Biochemical and genetic connection of At1 to NER
a–b, Coomassie-stained gel (left) and far-western blot (right) probed with FLAG-eAt1 (**a**) or FLAG-UvrA (**b**). **c**, MNNG-induced (top) and spontaneous (bottom) mutations of wild-type, *at11*, *rad13* and *at11 rad13* *S. pombe* strains. **d**, At11 and Rad13 are epistatic for MNNG toxicity. Serial dilutions of wild-type, *at11*, *rad13* and *at11 rad13* *S. pombe* cells spotted on yeast extract (YE) plates or YE plates containing 0.08 µg/ml MNNG. Results shown are mean ± s.d.; n = 3. **e–h**, Clonogenic assay, revealing At11 is epistatic for MNNG toxicity with Rad13 (**e**) and Swi10 (**f**), but not Rhp14 (**g**) or Rad2 (**h**). Results shown are mean ± s.e.m.; n = 3.

1 O^6 -Alkylguanine recognition by ATL



2 DNA bending and nucleotide flipping by ATL



3 ATL-dsDNA distortion recognition by NER proteins that wedge open dsDNA

4 Bubble incision and NER progression

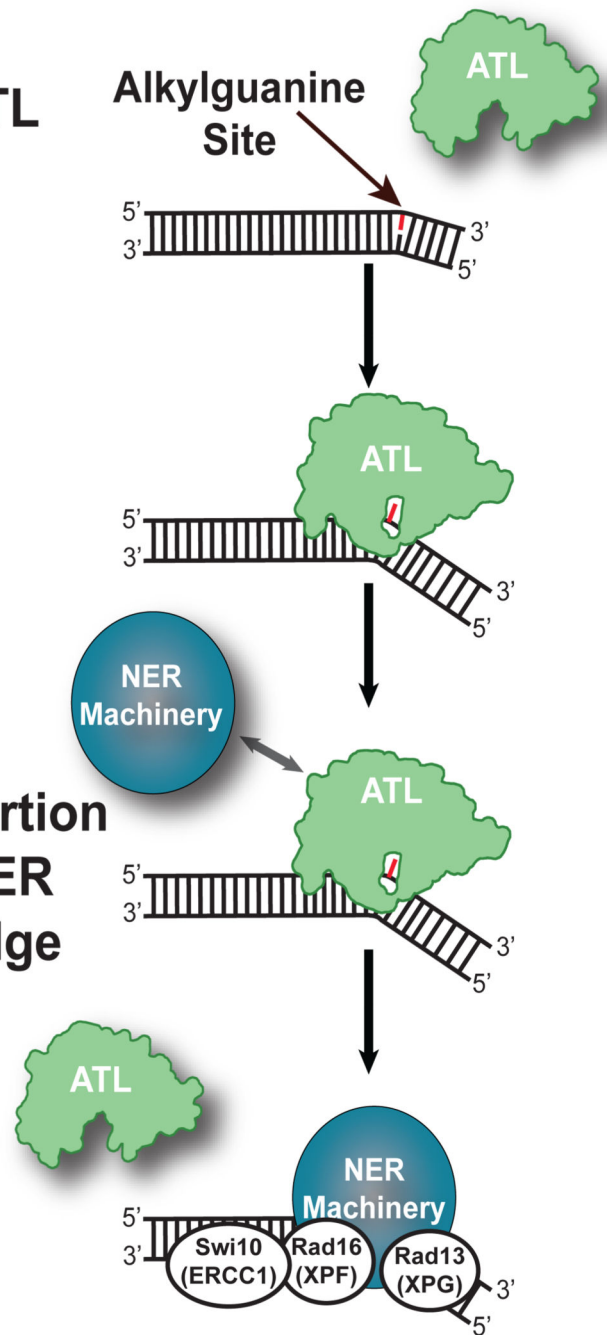


Figure 5. Alkyl-G lesion recognition allows NER repair of relatively non-distorting base lesions
 The distorted, stable ATL-DNA complex creates a platform to recruit NER enzymes to O^6 alkyl-G lesions. This general model is based upon our combined structural, biochemical and genetic results.